







Article

Sodar Observation of the ABL Structure and Waves over the Black Sea Offshore Site

Vasily Lyulyukin^{1,*} , Margarita Kallistratova¹ , Daria Zaitseva¹, Dmitry Kuznetsov¹, Arseniy Artamonov¹ , Irina Repina^{1,2} , Igor Petenko^{1,3} , Rostislav Kouznetsov^{1,4}  and Artem Pashkin^{1,2}

¹ A.M. Obukhov Institute of Atmospheric Physics, Moscow, Russia

² M.V. Lomonosov Moscow State University, Moscow, Russia

³ Institute of Atmospheric Sciences and Climate, Roma, Italy

⁴ Finnish Meteorological Institute, Helsinki, Finland

* Correspondence: lyulyukin@ifaran.ru

Abstract: The three-axes Doppler sodar Latan-3 operated on an oceanographic stationary platform in the coastal zone of the Black Sea in June 2015. The platform is located 450 meters offshore from the southern coast of the Crimea Peninsula in the region of Katsiveli (44.39° N, 33.99° E). The water depth at the site is about 30 meters. The atmospheric boundary layer (ABL) typical for the mediterranean seas was observed when the wind is from the sea. The physical processes typical for the coastal mountain terrain was observed when the wind was from the shore. Complex measurements of the ABL parameters were performed using a sodar. Auxiliary measurements of the ABL parameters were performed using a temperature profiler and an ultrasonic thermometer-anemometer. Observations were made mostly during a fair weather with a pronounced diurnal course of meteorological parameters. Sodar data analysis revealed a strong wave activity in the ABL. Internal gravity waves with amplitudes of up to one hundred meters were regularly observed in a layered turbulence structure under stable conditions. Various forms of Kelvin-Helmholtz billows were observed at the interface between the sea breeze and the return flow aloft and in the low level jets.

Keywords: breeze; sodar; atmospheric boundary layer; internal gravity waves; Kelvin-Helmholtz billows.

1. Introduction

Over the past two decades, several hundred studies of sea breezes were published. It is primarily caused by increased interest in wind power, although regional weather events and the spread of air pollutants in coastal zones remain important issues. The overwhelming majority of the publications are devoted to the numerical modeling (see e.g. [1–7]). At the same time, the number of experimental studies of sea breezes in various countries and regions has increased significantly as well. Thus, in the USA, recommendations on the development of meteorology for coastal/offshore wind energy for the next 10 years were adopted in 2013 [8], which noted the need for “continuous, publicly available, multilevel measurements of winds and temperature over offshore waters”.

A characteristic feature of experimental studies of sea breezes in recent years is the use of ground-based remote sensing as a supplement to conventional measurements. The sounding using radars [9], sodars [10], and lidars [11] made it possible to carry out studies of the vertical structure of sea breeze cells and fronts, encompassing return currents of the air. Ground-based remote sensing tools have been used for more than half a century in atmospheric research, and have provided a wealth of knowledge about the structure and dynamics of the atmospheric boundary layer (ABL) in various

locations and under various conditions [12]. For studying the lower part of the ABL the sodars, among the tools, are particularly suitable [13]. Sodars, along with measurements of wind speed components, allow visualizing mesoscale turbulent structures, including internal gravity waves, and determining their parameters. Recently, with the help of sodars, wave motions in a stable boundary layer (SBL) of midlatitudes [14–17] and in the Antarctic [18,19] were studied; the main types of observed waves, their periods and amplitudes were determined. However, until now, in the research of sea breezes sodars were used mainly as wind-profilers, without registration of the inner mesoscale structures (see, e.g. [20–24]). Only in a few sodar breeze studies some examples of internal gravity waves in breeze density currents were shown [25,26].

At the same time, the model calculations and laboratory experiments indicate a complex mesoscale structure of breezes, in particular, the presence of Kelvin-Helmholtz billows (KHB) in the breeze front region and in the interfaces between the forward and reverse breeze currents [27–31]. Such wavy structures are of considerable interest. First, KHB cause a friction-like force on the upper boundary of the air mass that slows the sea breezes inland progression [27,28]. Thus, they can influence the exchange processes in the density currents and, therefore, should be taken into account in the numerical models. Secondly, wave movements and short-term bursts can directly affect the efficiency of wind turbines in offshore farms [32,33]. In addition, high-frequency KHB can cause parasitic resonant oscillations of the hubs [34]. The above problems stimulate the study of waves and mesoscale turbulent structures in sea breezes.

This paper presents the results of a study of sea breezes in the northern part of the Black Sea, held in June 2015 during a two-week expedition of the A.M. Obukhov Institute of Atmospheric Physics, Russian Academy of Sciences. The highly sensitive mini-sodar, Latan-3M, installed on an oceanological platform in the offshore zone of the Crimea, served as the main measuring instrument. Note that in recent years, great attention has been paid to the sea breezes in the coastal zones of the Black Sea [35–39] due to the promising development of wind power in this region, which so far has only a small number of wind farms.

2. Measurement Site and Equipment

The studies were conducted at an oceanographic stationary platform in the coastal zone of the Black Sea in June 2015. The platform, managed by the Marine Hydrophysical Institute, is placed on the shelf slope of the southern coast of the Crimea Peninsula (44.39°N, 33.99°E, Figure 1(a)). The platform's location at a distance of approximately 450 m from the coast and the water depth about 30 m make it a unique observational point to collect data in the coastal zone in an area that is usually unresolved in remote sensing data sets. The coastline near the measurement site is significantly curved, with a small bay to the north. Near the platform (in the vicinity of 500 m), the coast extends from SW to NE direction; on a larger scale (up to 10 km), the coastline extends from WSW to ENE. With this shape of the coast, the early sea breeze is expected to have a SE direction perpendicular to the nearest coast edge, and then turn clockwise during the day due to enlargement and generalization of the breeze flow on the coast, and due to the influence of the Coriolis force.

The described picture, however, does not take into account the topography of the coastal slope, which can have a critical effect on the local wind. The platform is located offshore near the coast with a steep slope (in average about 200 m per 1 km distance) and a close location of the plateau (Figure 1(c)). A topographic profile of the coast extending north from the platform is presented in Figure 1(b). A neighborhood of the steep coast could lead to an occurrence of the katabatic and anabatic slope winds, which having the same direction as the breeze (during the day from the coast up the slope i.e. from sea to land, and at night from the mountain down to the coast, i.e. from the coast to the sea, like the night breeze), could ideally lead to a stronger breeze. A small glen runs north from the platform from the coast to the edge of the plateau, which can help establish a daily mountain-valley circulation with directions from the north at night and from the south during the day. But in general, the complex topography of the coast can also lead to the destruction of idealized breeze circulation.

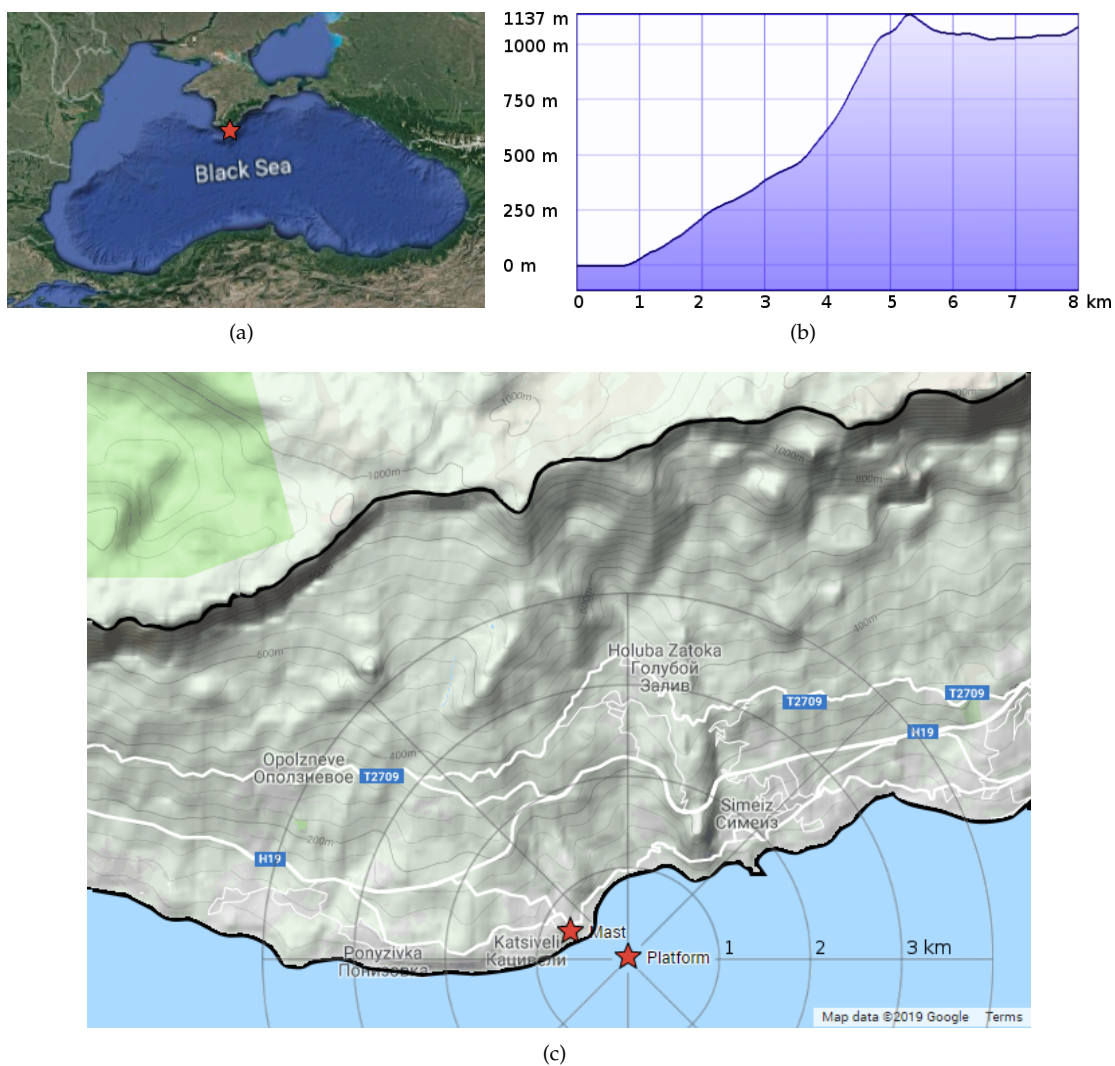


Figure 1. Experimental site location. (a) Location of the platform. (b) A topographic profile of the coast extending north from the platform. (c) Coastline topography near the platform. The coastline and the edge of plateau on the map are outlined with black lines.



Figure 2. General view of the platform (left) and sodar installation routine (right). Photos by Mikhail Varentsov and Dmitry Kuznetsov.

A general view of the platform is presented on Figure 2. The platform has several working levels. In order to minimize the effect of the platform constructions on measurements, the equipment was placed on the upper decks. We used the 3-beam Doppler sodar Latan-3m developed at the A.M. Obukhov Institute of Atmospheric Physics (Moscow, Russia) [40]. The sodar was operated with three 1.2-m dish antennas at sounding frequencies of 1.6–2.2 kHz. The operating mode with frequency-coded sounding pulse [41] and the parallel operation of the antennas were used to achieve high temporal resolution. The different frequency coding was used for the antennas to avoid cross talk: each antenna used an individual set of six frequencies emitted as a series of 50-ms pulses, which resulted in 10-m vertical resolution. The antennas were mounted on the iron flooring of the upper deck of the platform 14 meters above the sea level (a.s.l.), one vertically pointing and two inclined and directed to the open sea. Accordingly the lowest sounding level was 24 meters above the sea level. In Latan-3 sodars, the echo signal from each sounding is processed separately. The information on instantaneous signal and noise intensities and an along-beam radial wind speed component are stored for each of the three antennas range gate. During the campaign, the raw echo signals were stored as well for further reprocessing, should it be necessary.

The vertical temperature profiles up to 600 m were measured with a meteorological temperature profiler MTP-5 (by Research and Production Organization ATTEX) placed on the level 15 m a.s.l. facing the open sea. Near-surface standard meteorological measurements were provided by Vaisala Weather Transmitter WXT536 placed on the upper deck of the platform on a small meteorological masts at level 15 m a.s.l. Two Kipp&Zonen SMP21 pyranometers (280 to 3000 nm) and SGR3 pyrgeometers (4.4 to 50 μm) were operated on the platform to measure downward and upward shortwave and longwave radiation.

Measurements of meteorological parameters on the coast were carried out using the AIRMAR Weather Station, located on the meteorological mast on the roof of the building, 100 meters from the shore on the coastal slope. The height of the station above the ground level (a.g.l.) was 10 m, above the sea level - 45 m. The weather station was located 650 meters away to the north-west-west from the platform (Figure 1(c)).

3. Results

Sodar measurements on the platform were carried out in continuous mode from 12 to 22 June 2015, related measurements were provided most of this time period. The experiment was carried out mostly under fair weather conditions, and a pronounced diurnal course of meteorological parameters was observed. Predominantly stable and neutral stratification was observed over the sea surface. Convective plumes were observed on sodar echograms for less than 20% of time of measurements during offshore winds. The average relative humidity was about 70%, the maximum did not exceed 90%.

3.1. Diurnal Course of Meteorological Parameters

Figure 3 shows meteorological time series of synoptic observations and local measurement. The periods of cloudy weather were determined from measurements of longwave and shortwave radiation (Figure 3(a)), on the basis of method proposed by Marty and Philipona [42]. Variations of the apparent emittance due to cloud cover significantly exceed the variations of the clear sky emittance caused by variations of air humidity. We used the apparent emittance value as a criterion for determining cloudy periods. The threshold value of the emittance between clearsky and cloudy weather was chosen from the analysis of the time series of incoming shortwave radiation. In Figure 3 identified time periods of cloudy weather are marked by gray bars. The yellow bars indicate time periods of insolation according to measured shortwave downward radiation. Cloudy days (12, 17 and 19 June) were excluded from the statistics. Time series of air temperature measured at the platform mast 15 m a.s.l., at the onshore mast 10 m a.g.l. and water temperature are presented in Figure 3(b). Note, that during the entire experiment the water temperature did not exceed the air temperature at 15 m a.s.l. Time series of wind direction

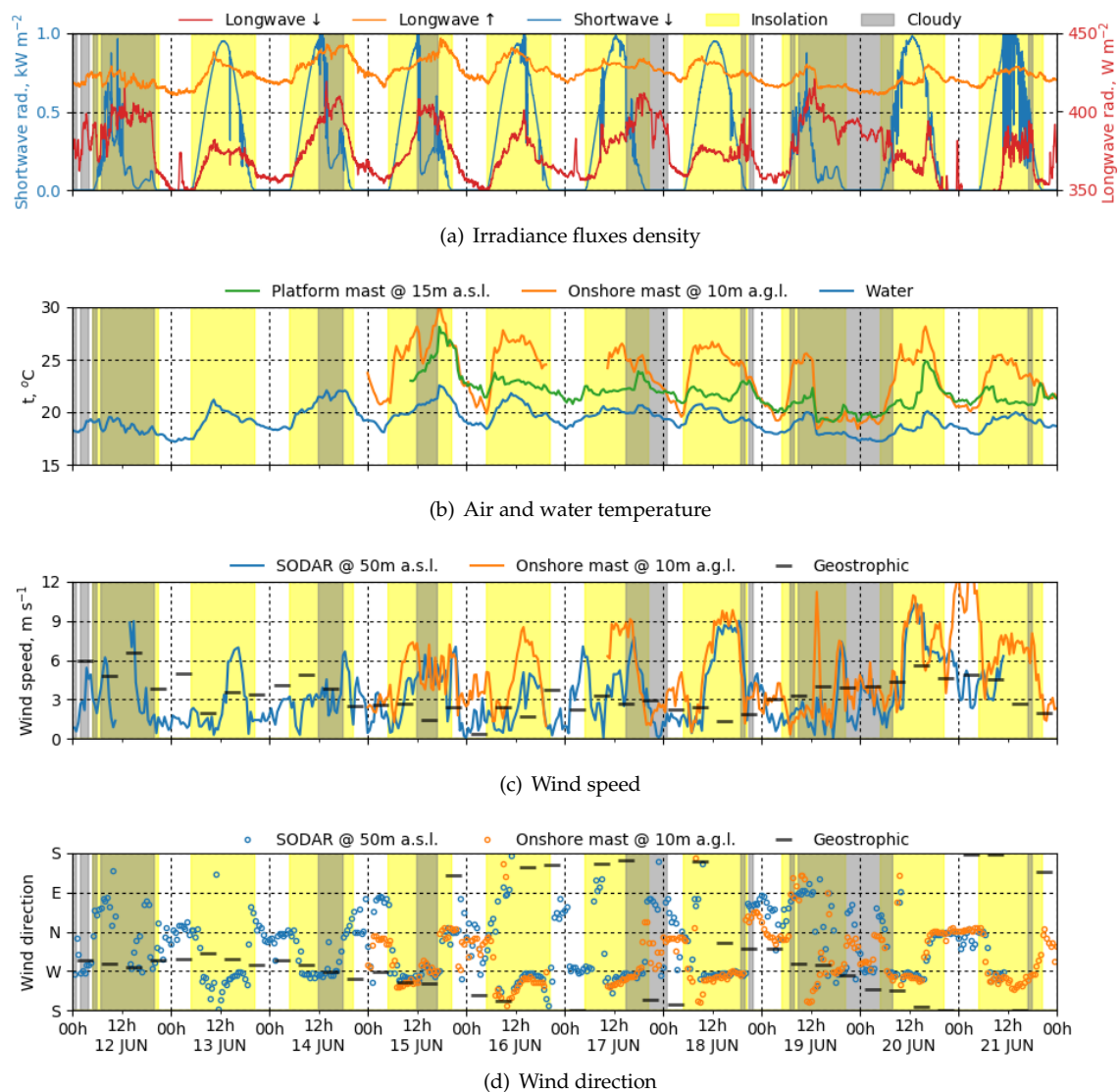


Figure 3. Meteorological time series of synoptic observations and local measurement. The gray bars indicate time periods of cloudy weather. The yellow bars indicate time periods of insolation. (a) Irradiance fluxes density. (b) Time series of air temperature at the platform mast 15 m a.s.l., at the onshore mast 10 m a.g.l. and water temperature. (c, d) Time series of wind speed and direction from the sodar at 50 m a.s.l., the onshore mast at 10 m a.g.l., and of synoptic wind at 10 m a.g.l. from reanalysis.

and speed from the data of sodar measurement and the onshore mast are presented in Figures 3(c) and 3(d). Steady west wind was observed daily in the daytime with speed values of up to 12 m s^{-1} at 50 m a.s.l. The night wind direction was less steady and generally ranged from the north-west to the east, with typical speed values of about $2\text{--}3 \text{ m s}^{-1}$ at 50 m a.s.l. A rapid change in wind direction in the morning and evening hours was observed daily. The values of geostrophic wind speed and direction, calculated from NCEP reanalysis data of sea level pressure are also presented in Figures 3(c) and 3(d). During the experiment geostrophic wind direction was predominantly western and ranged from the north-west to the south-east. According to a quadrant classification (see e.g. [43,44]) geostrophic wind direction was generally from quadrants Q1 and Q3. Scatter plots of wind speed and direction by sodar data for all days with fair weather presented in Figure 4. The plots show typical diurnal course of wind speed and direction with dominant direction from the north for night hours (from 19 to 7 o'clock) and from the west (along the coast) for daytime (from 7 to 19 o'clock).

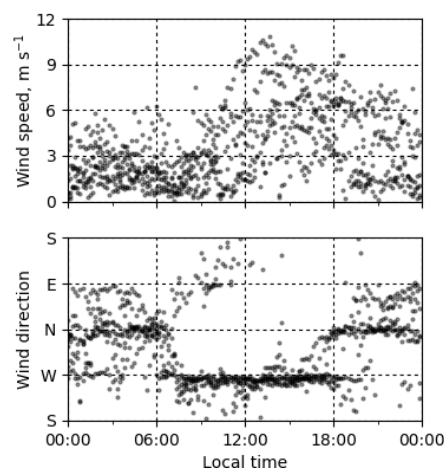


Figure 4. Diurnal time series of wind speed and wind direction from the sodar at 50 m a.s.l. for days with fair weather.

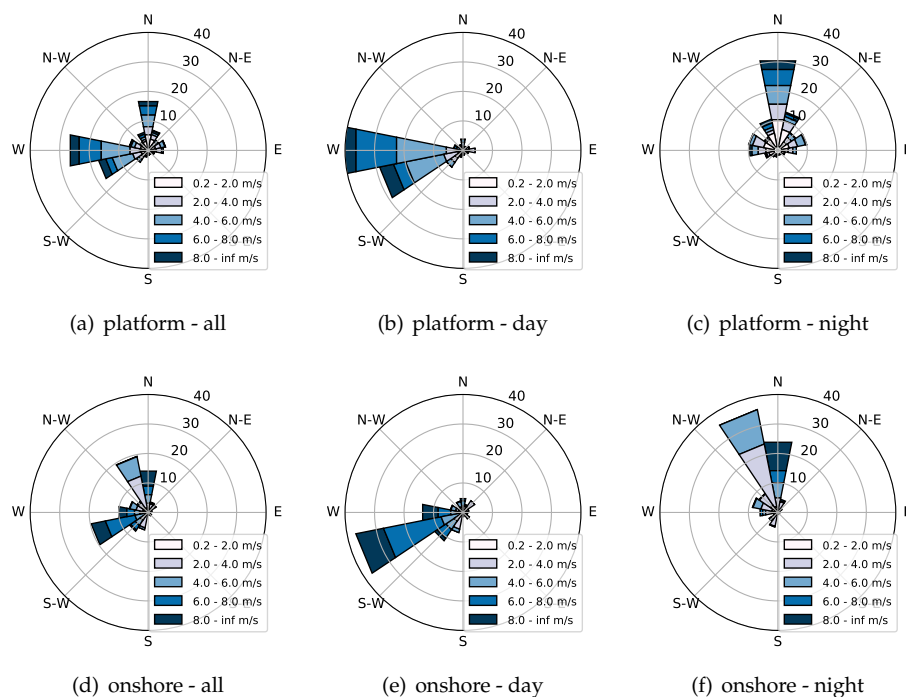


Figure 5. Wind roses near surface for days with fair weather. (a, b, c) Wind from platform mast 15 m a.s.l. (d, e, f) Wind from onshore mast 10 m a.g.l. Left panels correspond roses for all time, middle - for day hours (07–19 o'clock), right - for night hours (19–07 o'clock).

Wind roses from measurements at the platform and onshore masts for all days with fair weather are presented at Figure 5. Wind roses were built for the whole time and separately for day and night hours in accordance with the daily change of wind mode. The prevailing wind directions near the sea level were from the west (along the coast) and from the north (in the direction of the coastal slope). The north wind was typical for night time, west - for day time. Wind from the open sea (from the east) was observed sporadically in the morning hours and sometimes at night. The wind from the south was rare. The distribution of wind speed and direction according to measurements at the onshore mast qualitatively repeats the distribution of winds at the platform, however, a slight shift in the wind direction is observable, which can be associated with the orography of the area.

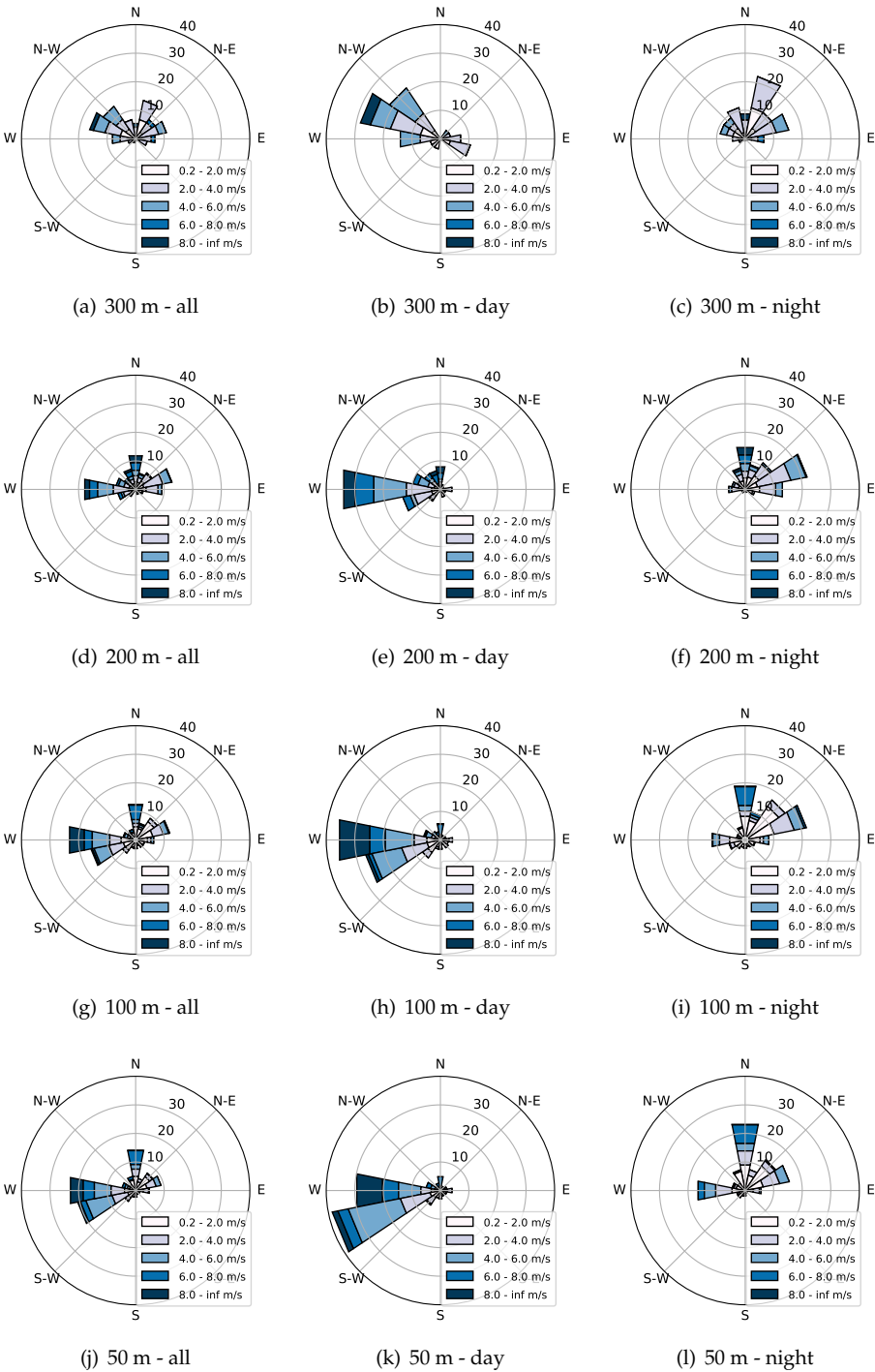


Figure 6. Windroses from sodar measurements for days with fair weather. Height levels are given relative to the sodar antennas placed at 15 m a.s.l.

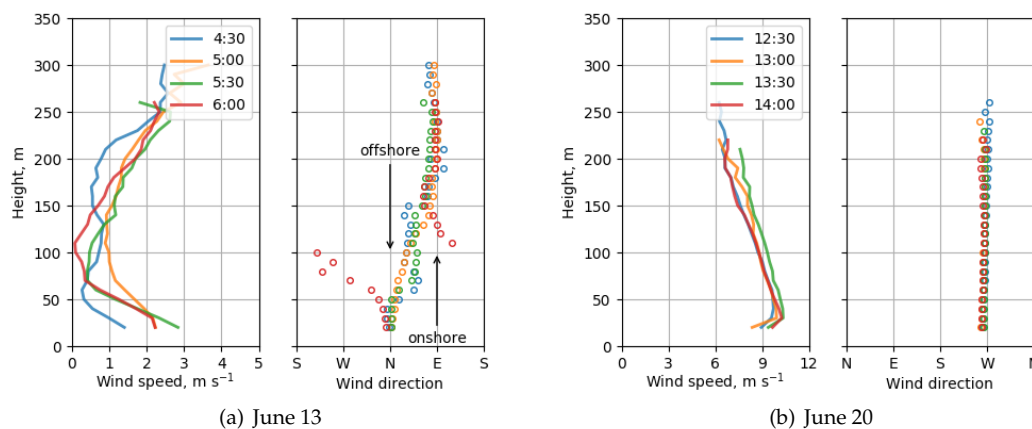


Figure 7. Time series of vertical profiles of wind speed and direction, which depict a permanent winds from the north (a) and west (b). Profiles are calculated with 30 minutes averaging.

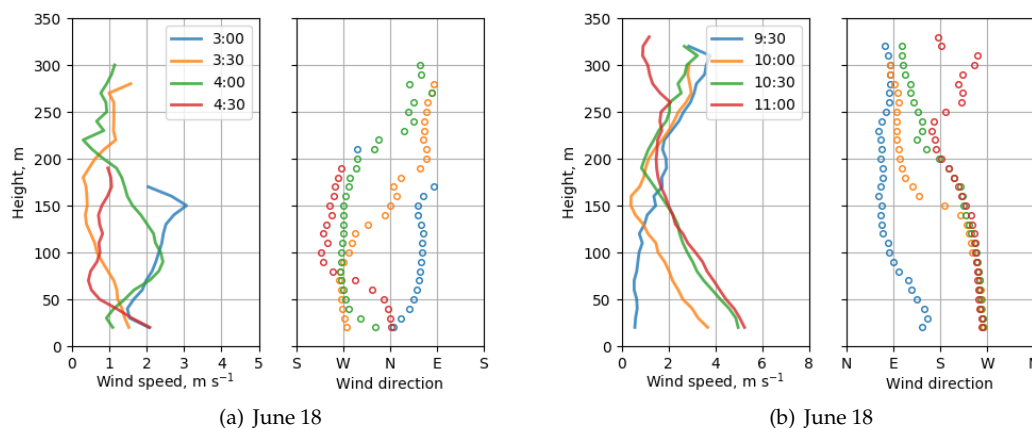


Figure 8. Time series of vertical profiles of wind speed and direction, which depict a volatile wind direction. Profiles are calculated with 30 minutes averaging.

3.2. Vertical Structure of the Wind Field

Wind roses from sodar data for various heights are presented in Figure 6. Height levels are given relative to the sodar antennas placed at 15 m a.s.l. The distribution of wind speed not significantly varies with height; however, there are systematic changes in the distribution of wind directions. Western winds, pronounced on the wind roses for daytime, turn clockwise with increasing altitude (which corresponds to the effect of Coriolis force). For night distribution, changing with height rather corresponds to the situation with a return breeze flow at heights above 100 m: the proportion of northern winds decreases with height and the fractions of winds with directions differing from northern one increase. At an altitude of 300 meters, the northern winds almost disappear. The change with height is not pronounced as one would expect in the case of classical breeze circulation. Southern winds are rare at all heights. It is important to note that the sodar wind rose at 300 m is not fully representative, since the altitude range of sounding depends significantly on meteorological conditions, and wind speed data at 300 m were available for less than 30% of the time, mainly for winds from the shore.

Figures 7 and 8 show examples of time series of vertical profiles of wind speed and direction characterizing the typical vertical structure of the wind field. Profiles are calculated with 30 minutes averaging. Examples of regular and stable wind conditions are presented in Figure 7. Figure 7(a) shows

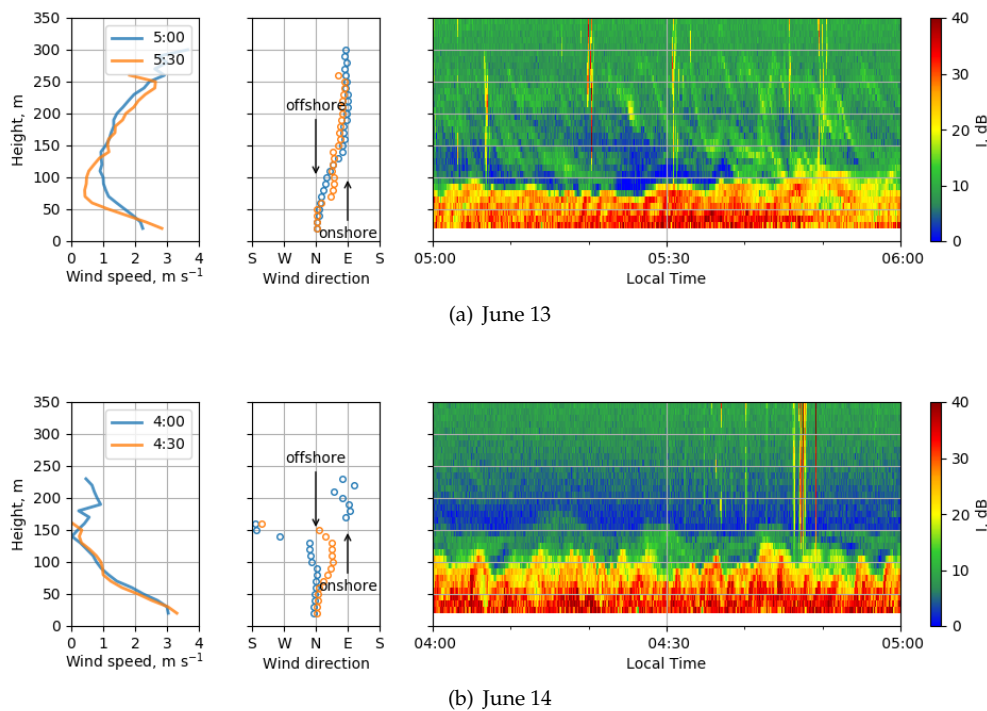
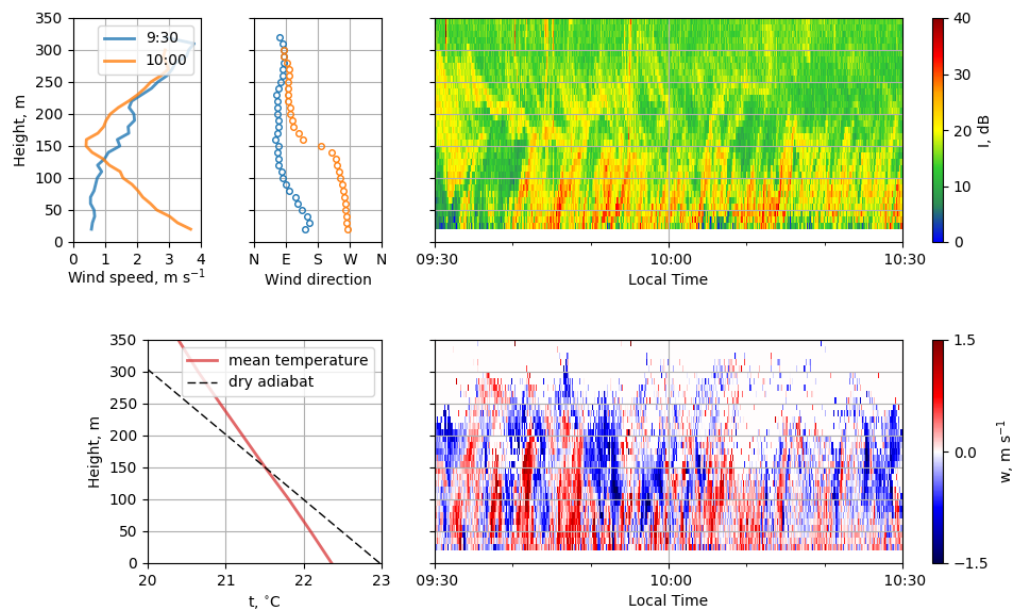


Figure 9. Two episodes of KHB observation in the nocturnal boundary layer under the north wind (offshore) near the sea surface, and a return flow aloft (onshore). For each episode left panels present vertical profiles of wind speed and direction, right panels present return signal in height–time coordinates (echograms), colors show the relative intensity of sodar return signal. Profiles are calculated with 30 minutes averaging. Note the opposite orientation of the billows in the lower and upper parts of the echogram in episode (a).

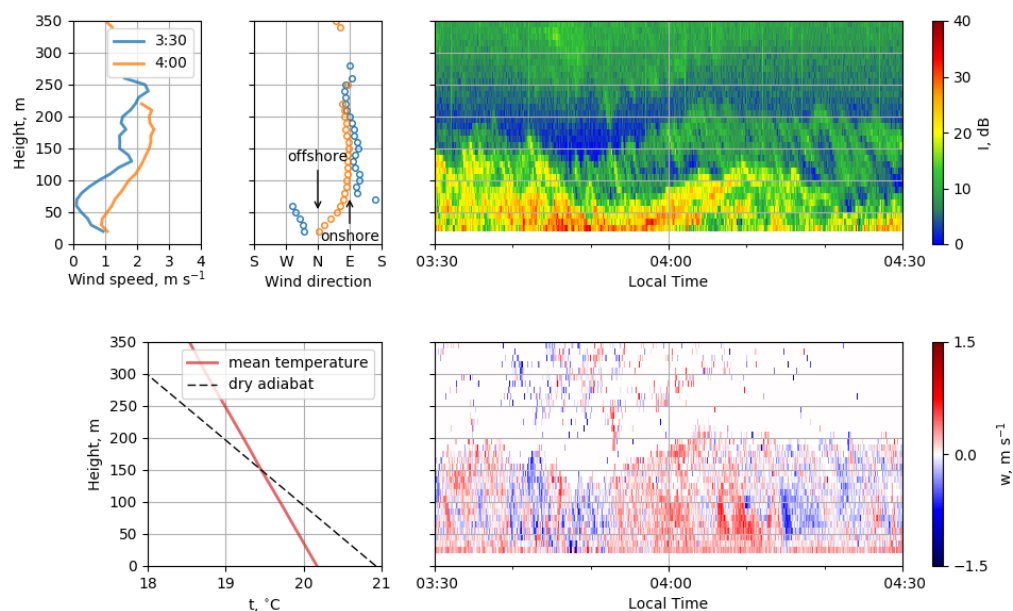
profiles for the situation of northern wind near the sea surface at night. The wind direction changes from the north (offshore direction) to the east (onshore direction) with the height passing through a minimum at an altitude of about 100 m. Both clockwise and counterclockwise (by 270 degrees) rotations are presented. The lower part of the profiles corresponds to the picture of a low-level jet (LLJ) stream with a maximum speed of about $3\text{--}4\text{ m s}^{-1}$, located below the sounding range. Figure 7(b) shows an example of a steady west wind observed in the daytime. Wind direction almost does not change with height. The wind speed profile corresponds to a LLJ stream with a maximum wind speed of up to 11 m s^{-1} located below 50 meters. In the absence of a steady western wind, frequent changes in the wind direction near the sea surface by 90 degrees or more were observed. In this case, as a rule, the change in wind direction did not occur simultaneously at different heights, forming volatile vertical profiles, characterized by significant vertical wind shears. Figure 8 shows profiles series for cases of changing of the wind direction near the sea surface, accompanied by rotation of the wind with height.

3.3. Observation of Wave Structures in Shear Flows

Under stable ABL stratification, the presence of vertical wind shear in the layer can lead to the Kelvin-Helmholtz instability and cause the formation of Kelvin-Helmholtz billows (KHB). During the experiment such turbulent structures in the form of braids or inclined stripes were regularly observed in sodar echograms. Sodar return signal is proportional to structural parameter C_T^2 in the inertial interval [45], and therefore can be considered as a measure of turbulence. Figures 9 and 10 show examples of such observations. Figure 9 shows a series of wind speed and direction profiles, and sodar echograms for two episodes of observation of KHB in the nocturnal boundary layer under the north



(a) June 18



(b) June 18

Figure 10. KHB episodes observed by sodar matching the temperature stratification (bottom left panels) and vertical velocity field (bottom right panels). Wind profiles are calculated with 30 minutes averaging. Temperature profiles are calculated with 60 minutes averaging.

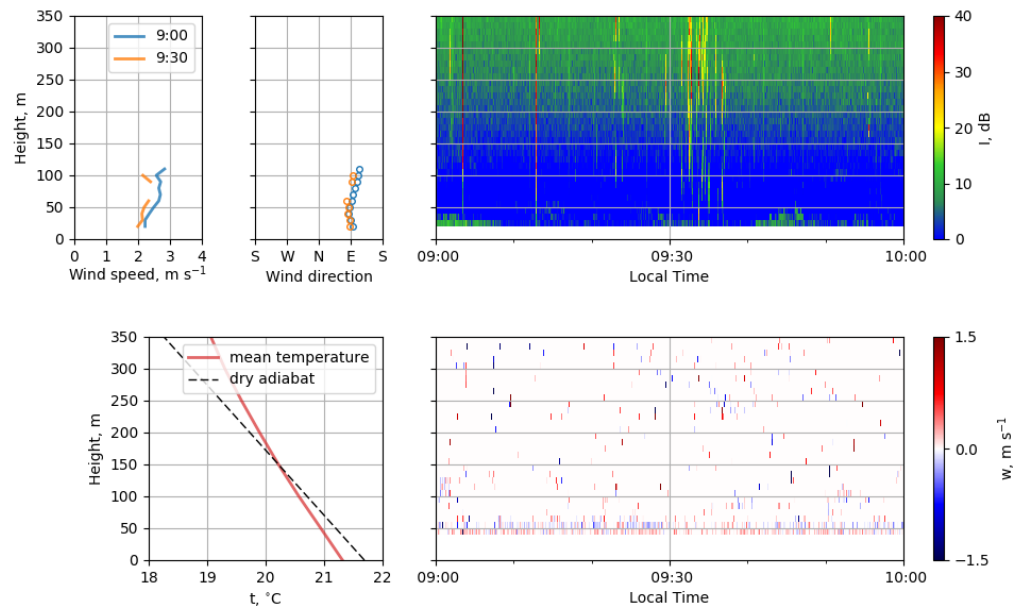
wind near the sea surface, changing to the east direction (onshore) with height. In the cases presented, in the lower layer of up to 100 m, there is a negative wind speed shear (about 4 m s^{-1} per 100 m) in the presence of LLJ with a maximum below the sounding range. In the field of scattered signal in the lower turbulent layer, wave structures are observed in the form of braid tilted to the right. Time period of observed structures was about 2 minutes, which equals (corresponding to the Taylor hypothesis of frozen turbulence) about 250 m to the space period. On the echogram in Figure 9(a) KHB in the form of braid tilted to the left are observed in the layer with a positive wind speed shear above the level of the minimum wind speed. The quazi period of the KHB is about 3–5 min (400–600 m) and the double amplitude of the wave (equal to thickness of the wavy layer) is about 150 m. Such shapes with the opposite inclination of the braids correspond to the typical KHB structures in shear flows with different signs of shear [46].

Kelvin-Helmholtz billows can lead to an increase in vertical heat and mass transfer due to the generation of turbulence [47]. Indirectly, the degree of vertical exchange can be judged by a vertical velocity field. Figure 10 shows examples of matching of the echograms with the registration of KHB structures on sodar echograms with the two-dimensional fields of vertical velocity. A series of vertical profiles of wind speed and direction by sodar and temperature profile by the profiler are also presented in Figure 10. Dry adiabats are shown to estimate temperature stratification. Figure 10(a) shows a matching for the case of wind direction changing from west to east with height. Two wave layers can be observed. In the lower layer up to 150 m with a negative wind shear (about 2 m s^{-1} per 100 m) a wavy structure is observed as a series of quasi-periodic stripes inclined to the right, in the upper layer from 150 m to 300 m with a positive shear (about 2 m s^{-1} per 100 m) - as stripes tilted to the left. Time period of observed structures was about 2 minutes, which equals to a space period of about 250 m. In the fields of vertical velocity presented, alternating areas of ascending and descending flows are visible matching the shape of turbulent structures in the field of the sodar return signal. Figure 10(b) shows a matching for the case of a complex KHB structure in several layers with time periods from 1 to 3 minutes.

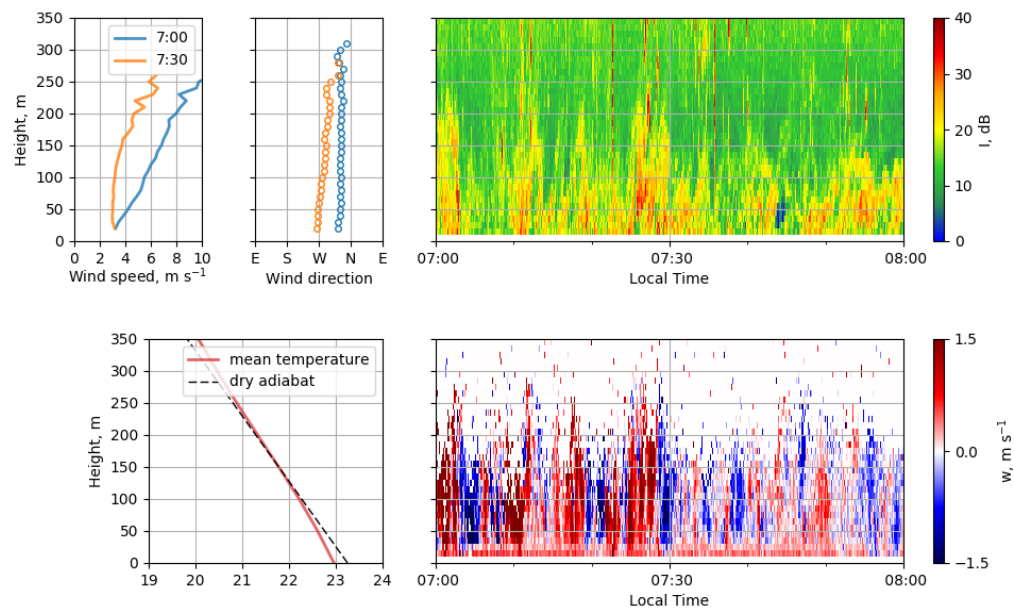
For comparison, Figure 11 shows echograms and vertical wind speed fields for the case of low level of turbulence (surface turbulent layer is lower than the sodar sounding range) with the wind from the sea (Figure 11(a)) and the case of intense convection brought by the north wind from the land (Figure 11(b)).

4. Discussion

During the experiment, a pronounced daily course of the wind field was observed, also accompanied by various sporadic changes in the wind direction near the sea surface. The experiment did not observe the breeze circulation in the “pure” form. Cases of a violent change in wind direction with height similar to breeze return flow pattern were observed rarely enough. Usually such episodes were lasting no more than 3 hours, and the wind direction in the return flow was volatile. A steady west wind observed in the daytime (and sometimes at night, for example, 17 June from 0 to 7 o’clock), changes direction slightly and has a maximum speed of 12 m s^{-1} (at 50 meters a.s.l.) which is difficult to explain with a pure breeze circulation. Most likely, multiple factors acted simultaneously: thermal pressure gradient, synoptic wind, and orographic features of the coast. When geostrophic wind direction is from quadrants Q1 or Q3, the daytime thermal pressure gradient should lead to an increase of along-shore component of near-surface wind (W-SWW in our case). Geostrophic wind from Q1 is also favorable for the development of “corkscrew” sea breeze [28,43]. Nocturnal offshore wind flow accompanied by a change of direction to the east (from the open sea sector) at an altitude of about 200 m can be conditionally attributed to the enhance of the night breeze by the katabatic flow. The night wind flow was less steady and noticeably weaker then the daytime wind, and had a typical speed values of about $2\text{--}3 \text{ m s}^{-1}$ at 50 m a.s.l. Sometimes wind direction from the east was observed on the platform, when the north wind was observed at the onshore mast.



(a) June 19



(b) June 21

Figure 11. Episodes representing low turbulence (a) and convection (b) conditions. Wind profiles are calculated with 30 minutes averaging. Temperature profiles are calculated with 60 minutes averaging.

Comparison of the wind direction and speed in the lower part of the ABL with wind data for this site described in literature [35,48] shows that the observed pattern of wind distribution is quite representative for this area in summer season. Numerical modeling of the breeze for this region [37] gives average values of the wind speed about $1\text{--}2\text{ m s}^{-1}$ and SW and NE direction for the day and night breeze respectively, at time of maximum development for summer season. The simulated wind velocity fields demonstrate that in the region of the Southern coast of the Crimean peninsula, the day and night breezes over the sea are primarily determined by small-scale inhomogeneities of the coast and by adjacent mountains. The day breeze is blocked by quite high Crimean mountains, and the night breeze has the character of a katabatic flow from the mountain range. It has also been shown that the night breeze, on the whole, has less power than the day breeze due to lower temperature gradients. However, the spatial resolution of the modeling results presented in [37] is too low (about 0.02 degrees) for a detailed comparison with the observational data.

The shape and structure of the KHB observed in the shear flows during the experiment coincide with the previous studies of KHB described by the authors [49,50]. The periods of the waves are consistent with the results of sodar observations of breezes in [26]. The cases of simultaneous observation of two wave layers with different inclination of KHB is similar to those described in paper [51], but with the opposite orientation of the tilts. Note that the KHB were observed in the form of short (merely several periods of wave) trains in contrast to KHB in low-level jet streams over a uniform land, where KHB trains of several hours were observed [15]. This corresponds to the overall strong and rapid variability of the mesoscale sea breeze pattern recorded in our experiment.

Violent changes of wind direction with height have a significant effect on the stability of stratification in the layer due to shear instability. The wide variety of observed wind speed and direction profiles and their frequent and unpredictable change make it difficult to predict dynamical stability conditions. Statistical analysis of long time series of remote sensing observations, organized with regard to local features of the coastline, is necessary for their description. To assess the effect of synoptic conditions, an analysis of long time series of continuous observations is also necessary.

5. Conclusions

For the first time, sodar measurements of ABL parameters were carried out in the coastal zone of the northern part of the Black Sea. During 10 days in June 2015, the three-axis Doppler sodar operated on a stationary oceanographic platform located at a distance of 450 m from the coastline. This made it possible to investigate vertical profiles of wind speed and direction, as well as mesoscale wave structures in the sea breeze flows.

Steady west wind was observed daily in the daytime with speed values of up to 12 m s^{-1} at 50 m a.s.l. The night wind was less steady and noticeably weaker, with typical speed values of about $2\text{--}3\text{ m s}^{-1}$ at 50 m a.s.l. A rapid change in wind direction in the morning and evening hours was observed daily. Return air flow aloft was rarely observed at altitudes of 200–300 m. A characteristic feature of the winds in the studied area was a typical difference of about 90° between night and day near-surface flows. The main direction of the daytime wind at all heights was from the SW–W sector. The night wind did not blow from the opposite direction, but from the N–NE sector, rarely from NW–N. The night wind was mainly determined by the katabatic air flow from the slopes of the coastal mountain range.

A visual analysis of sodar echograms revealed many episodes of wave activity in the ABL over the coastal zone. A short trains of Kelvin-Helmholtz billows in the form of braids were observed usually at dawn in the upper part of the onshore sea breeze flow, i.e. at altitudes where the wind speed fell with altitude. The KHB periods were 2–4 min. In some cases, the KHB with periods of 7–8 min were also observed in the lower part of the return flow, in layer with a positive the wind speed shear. The inclination of billows in the lower and upper flows was opposite.

Based on our short-term measurements, the coastal strip of the studied area seems to be unsuitable for the wind energy use, due to the low mean wind speed, its strong variability and the strong

intermittency of mesoscale and wave structures in the turbulence and wind speed. However, for comprehensive inference, long-term experimental studies in different seasons are needed.

Author Contributions: Conceptualization, V.L., M.K., I.R. and I.P.; Data curation, V.L., D.Z., D.K. and I.R.; Formal analysis, V.L., D.Z., A.A. and A.P.; Funding acquisition, M.K. and I.R.; Investigation, V.L., D.K. and A.A.; Methodology, V.L., M.K. and R.K.; Project administration, I.R.; Resources, V.L., D.K., A.A., I.R. and R.K.; Software, V.L. and R.K.; Supervision, M.K.; Validation, V.L., D.Z. and R.K.; Visualization, V.L. and D.Z.; Writing – original draft preparation, V.L.; Writing – review and editing, M.K. and I.P.

Funding: This research was funded by the Russian Foundation for Basic Research through grant number 19-05-01008; the expedition was organized in the framework of project of Russian Science Foundation number 14-27-00134; processing and analysis of turbulent measurement data were carried out with the support of Russian Science Foundation through grant number 17-17-01210.

Acknowledgments: The authors are grateful to Otto Chkhetiani for help in organizing the expedition and Valerii Kramar for data of measurements by the weather station at the onshore mast. NCEP Reanalysis data provided by the NOAA/OAR/ESRL PSD, Boulder, Colorado, USA, from their Web site at <https://www.esrl.noaa.gov/psd/>

Conflicts of Interest: The authors declare no competing interests. The funders had no role in the design of the study; in the collection, analyses, or interpretation of data; in the writing of the manuscript, or in the decision to publish the results.

Abbreviations

The following abbreviations are used in this manuscript:

ABL	atmospheric boundary layer
a.s.l.	above the sea level
a.g.l.	above the ground level
KHB	Kelvin-Helmholtz billows
LLJ	low-level jet

References

1. Crosman E.T., H.J. Sea and Lake Breezes: A Review of Numerical Studies. *Boundary-Layer Meteorol.* **2010**, *137*, 1–29. doi:10.1007/s10546-010-9517-9.
2. Salvador, N.; Reis, N.C.; Santos, J.M.; Albuquerque, T.T.A.; Lariato, A.G.; Delbarre, H.; Augustin, P.; Sokolov, A.; Moreira, D.M. Evaluation of weather research and forecasting model parameterizations under sea-breeze conditions in a North Sea coastal environment. *Journal of Meteorological Research* **2016**, *30*, 998–1018.
3. Huang, Q.; Cai, X.; Song, Y.; Kang, L. A numerical study of sea breeze and spatiotemporal variation in the coastal atmospheric boundary layer at Hainan Island, China. *Boundary-Layer Meteorology* **2016**, *161*, 543–560. doi:10.1007/s10546-016-0177-2.
4. Olsen, B.T.; Hahmann, A.N.; Sempreviva, A.M.; Badger, J.; Jørgensen, H.E. An intercomparison of mesoscale models at simple sites for wind energy applications. *Wind Energy Sci* **2017**, *2*, 211–228.
5. Salvação N., S.C.G. Wind resource assessment offshore the Atlantic Iberian coast with the WRF model. *Energy* **2018**, *145*, 276–287.
6. Banta, R.B.; Pichugina, Y.L.; Brewer, W.A.; James, E.P.; Olson, J.B.; Benjamin, S.G.; Carley, J.R.; Bianco, L.; Djalalova, I.V.; Wilczak, J.M.; Hardesty, R.M.; Cline, J.; Marquis, M.C. Evaluating and Improving NWP Forecast Models for the Future: How the Needs of Offshore Wind Energy Can Point the Way. *Bulletin of the American Meteorological Society* **2018**, *99*, 1155–1176.
7. Prósper, M.A.; Otero-Casal, C.; Fernández, F.C.; Miguez-Macho, G. Wind power forecasting for a real onshore wind farm on complex terrain using WRF high resolution simulations. *Renewable Energy* **2019**, *135*, 674–686.
8. Archer, C.L.; Colle, B.A.; Delle Monache, L.; Dvorak, M.J.; Lundquist, J.; Bailey, B.H.; Beaucage, P.; Churchfield, M.J.; Fitch, A.C.; Kosovic, B.; others. Meteorology for coastal/offshore wind energy in the United States: recommendations and research needs for the next 10 years. *Bulletin of the American Meteorological Society* **2014**, *95*, 515–519. doi:10.1175/BAMS-D-13-00108.1.

9. Suresh, R. Observation of Sea Breeze Front and its Induced Convection over Chennai in Southern Peninsular India Using Doppler Weather Radar. *Pure Appl. Geophys.* **2007**, *164*, 1511–1525. doi:10.1007/s00024-007-0234-3.
10. Maksymova, N. The Black Sea breezes as seen with sodar and RASS. *Telecommunications and Radio Engineering* **2011**, *70*, 899–915. doi:10.1615/TelecomRadEng.v70.i10.50.
11. Tuononen, M.; O'Connor, E.J.; Sinclair, V.A.; Vakkari, V. Low-level jets over Utö, Finland, based on Doppler lidar observations. *J. Appl. Meteorol. Climatol.* **2017**, *56*, 2577–2594.
12. Wilczak, J.; Gossard, E.; Neff, W.; Eberhard, W. Ground-based remote sensing of the atmospheric boundary layer: 25 years of progress. *Bound.-Layer Meteorol.* **1996**, *78*, 321–349.
13. Coulter, R.L.; Kallistratova, M.A. The Role of Acoustic Sounding in a High-Technology Era. *Meteorology and Atmospheric Physics* **1999**, *71*, 3–13.
14. Lyulyukin, V.S.; Kallistratova, M.A.; Kouznetsov, R.D.; Kuznetsov, D.D.; Chunchuzov, I.P.; Chirokova, G.Y. Internal Gravity-Shear Waves in the Atmospheric Boundary Layer by the Acoustic Remote Sensing Data. *Izvestia, Atmospheric and Oceanic Physics* **2015**, *51*, 193–202.
15. Kallistratova, M.A.; Lyulyukin, V.S.; Kouznetsov, R.D.; Petenko, I.V.; Zaitseva, D.V.; Kuznetsov, D.D. Sodars Studies of Kelvin-Helmholtz Billows in the Low-Level Jets. In *Dynamics of Wave and Exchange Processes in the Atmosphere*; Chkhetiani, O.; Gorbunov, M.; Kulichkov, S.; Repina, I., Eds.; GEOS: Moscow, 2017; pp. 212–259.
16. Zaitseva, D.V.; Kallistratova, M.A.; Lyulyukin, V.S.; Kouznetsov, R.D.; Kuznetsov, D.D. The Effect of Internal Gravity Waves on Fluctuations in Meteorological Parameters of the Atmospheric Boundary Layer. *Izvestiya Atmospheric and Oceanic Physics* **2018**, *54*, 173–181.
17. Kallistratova, M.A.; Petenko, I.V.; Kouznetsov, R.D.; Kulichkov, S.N.; Chkhetiani, O.G.; Chunchusov, I.P.; Lyulyukin, V.S.; Zaitseva, D.V.; Vazaeva, N.V.; Kuznetsov, D.D.; Perepelkin, V.G.; Bush, G.A. Sodar Sounding of the Atmospheric Boundary Layer: Review of Studies at the Obukhov Institute of Atmospheric Physics, Russian Academy of Sciences // *Izvestiya. Atmospheric and Oceanic Physics* **2018**, *54*, 242–256. doi:10.1134/S0001433818030088.
18. Petenko, I.; Argentini, S.; Casasanta, C.; Kallistratova, M.; Sozzi, R.; Viola, A. Wavelike Structures in the Turbulent Layer During the Morning Development of Convection at Dome C, Antarctica. *Boundary-Layer Meteorol.* **2016**, *161*, 289–307. doi:10.1007/s10546-016-0173-6.
19. Petenko, I.; Argentini, S.; Casasanta, C.; Genthon, C.; Kallistratova, M. Stable Surface-Based Turbulent Layer During the Polar Winter at Dome C, Antarctica: Sodar and In Situ Observations. *Boundary-Layer Meteorology* **2019**, *171*, 101–128. doi:10.1007/s10546-018-0419-6.
20. Mastrantonio, G.; Petenko, I.; Viola, A.P.; Argentini, S.; Coniglio, L.; Monti, P.; Leuzzi, G. Influence of the synoptic circulation on the local wind field in a coastal area of the Tyrrhenian Sea. *IOP Conf. Series: Earth and Environmental Science* **2008**, *1*. doi:10.1088/1755-1307/1/1/012049.
21. Federico, S.; Pasqualoni, L.; DeLeo, L.; Bellecci, C. A study of the breeze circulation during summer and fall 2008 in Calabria Italy. *Atmospheric Research* **2010**, *97*, 1–13. doi:10.1016/j.atmosphere.2010.02.009.
22. Helmis, C.G.; Wang, Q.; Sgouros, G.; Wang, S.; Halios, C. Investigating the summertime low-level jet over the East Coast of the USA: A case study. *Bound.-Layer Meteorol.* **2013**, *149*, 259–276. doi:10.1007/s10546-013-9841-y.
23. Calmet, I.; Mestayer, P.G. Study of the thermal internal boundary layer during sea-breeze events in the complex coastal area of Marseille. *Theor. Appl. Climatol.* **2016**, *123*, 801–826. doi:10.1007/s00704-015-1394-1.
24. Barantiev, D.; Batchvarova, E.; Novitsky, M. Breeze circulation classification in the coastal zone of the town of Ahtopol based on data from ground based acoustic sounding and ultrasonic anemometer. *Bulgarian Journal of Meteorology and Hydrology* **2017**, *22*, 2–25.
25. Chiba, O. Variability of the sea-breeze front from SODAR measurements. *Boundary-Layer Meteorology* **1997**, *82*, 165–174.
26. Rakesh, P.; Sandeepan, B.S.; Venkatesan, R.; Baskaran, R. Observation and numerical simulation of submesoscale motions within sea breeze over a tropical coastal site: A case study. *Atmospheric Research* **2017**, *198*, 205–215. doi:10.1016/j.atmosres.2017.08.006.
27. Simpson, J.E.; Mansfield, D.A.; JR., M. Inland penetration of sea-breeze fronts. *Quarterly Journal of the Royal Meteorological Society* **1977**, *103*, 47–76. doi:10.1002/qj.49710343504.

28. Miller, S.T.K.; Keim, B.D.; Talbot, R.W.; Mao, H. Sea breeze: structure, forecasting, and impacts. *Reviews of Geophysics* **2003**, *41*. doi:10.1029/2003rg00012.
29. Sha, W.; Ogawa, S.; Iwasaki, T.; Wang, Z. A Numerical Study on the Nocturnal Frontogenesis of the Sea-breeze Front. *Journal of the Meteorological Society of Japan* **2004**, *82*, 817–823. doi:10.2151/jmsj.2004.817.
30. Plant, R.S.; Keith, G.J. Occurrence of Kelvin-Helmholtz Billows in Sea-breeze Circulations. *Boundary-Layer Meteorology* **2007**, *122*, 1–15. doi:10.1007/s10546-006-9089-x.
31. Feliks, Y.; Tziperman, E.; Farrell, B. Non-normal growth of Kelvin-Helmholtz eddies in a sea breeze. *Q.J.R.Meteorol.Soc.* **2014**, *140*, 2147–2157. doi:10.1002/qg.2285.
32. Smith, R.B. Gravity wave effects on wind farm efficiency. *Wind Energy* **2010**, *13*, 449–458.
33. Ollier, S.J.; Watson, S.J.; Montavon, C. Atmospheric gravity wave impacts on an offshore wind farm. *Journal of Physics: Conference Series* **2018**, *1037*, 072050. doi:10.1088/1742-6596/1037/7/072050.
34. Hand, M.M. Mitigation of Wind Turbine/Vortex Interaction Using Disturbance Accommodating Control. Technical report, Report NREL/TP-500-35172, 2003.
35. Pospelov, M.; Biasio, F.D.; Goryachkin, Y.; Komarova, N.; Kuzmin, A.; Pampaloni, P.; Repina, I.; Sadovsky, I.; Zecchetto, S. Air-sea interaction in a coastal zone: The results of the CAPMOS'05 experiment on an oceanographic platform in the Black Sea. *Atmospheric Research* **2009**, *94*, 61–73. doi:10.1016/j.atmosres.2009.02.002.
36. Barantiev, D.; Novitsky, M.; Batchvarova, E. Meteorological observations of the coastal boundary layer structure at the Bulgarian Black Sea coast, *Adv. Sci. Res* **2011**, *6*, 251–259. doi:10.5194/asr-6-251-2011.
37. Efimov, V.V.; Krupin, A.V. Breeze Circulation in the Black Sea Region. *Russian Meteorology and Hydrology* **2016**, *41*, 240–246.
38. Davy, R.; Gnatiuk, N.; Pettersson, L.; Bobylev, L. Climate change impacts on wind energy potential in the European domain with a focus on the Black Sea. // *Renew. Sustain. Energy Rev* **2018**, *2018*, 1652–1659.
39. Rusu, E.A. 30-year projection of the future wind energy resources in the coastal environment of the Black Sea. *Renew. Energy* **2019**, *139*, 228–234.
40. Kouznetsov, R. LATAN-3 sodar for investigation of the atmospheric boundary layer. *Atm. and Oceanic Opt.* **2007**, *20*, 684–687.
41. Kouznetsov, R.D. The multi-frequency sodar with high temporal resolution. *Meteor. Zeitschrift* **2009**, *18*, 169–173. doi:10.1127/0941-2948/2009/0373.
42. Marty, C.; Philipona, R. The clear-sky index to separate clear-sky from cloudy-sky situations in climate research. *Geophysical Research Letters* **2000**, *27*, 2649–2652.
43. Adams, E. Four ways to win the sea breeze game. *Sailing World* **1997**, *3*, 44.
44. Mestayer, P.G.; Calmet, I.; Herlédant, O.; Barré, S.; Piquet, T.; Rosant, J.M. A coastal bay summer breeze study, part 1: results of the Quiberon 2006 experimental campaign. *Boundary-layer meteorology* **2018**, *167*, 1–26.
45. Tatarskii, V.I. The effects of the turbulent atmosphere on wave propagation. *Jerusalem: Israel Program for Scientific Translations*, 1971 **1971**.
46. Muschinski, A. Possible effect of Kelvin-Helmholtz instability on VHF radar observation of the mean vertical wind. *J. Appl. Meteorology* **1996**, *35*, 2210–2217.
47. Sun, J.; Mahrt, L.; Nappo, C.; Lenschow, D.H. Wind and temperature oscillations generated by wave-turbulence interactions in the stably stratified boundary layer. *J. Atmos. Sci.* **2015**, *72*, 1484–1503.
48. Repina, I.; Artamonov, A.; Varentsov, M.; Kozyrev, A. Experimental Study of High Wind Sea Surface Drag Coefficient. *Physical Oceanography* **2015**. doi:10.22449/1573-160x-2015-1-49-58.
49. Lyulyukin, V.; Kouznetsov, R.; Kallistratova, M. The Composite Shape and Structure of Braid Patterns in Kelvin-Helmholtz Billows Observed with a Sodar. *Journal of Atm. and Ocean. Tech.* **2013**, *30*, 2704–2711. doi:10.1175/JTECH-D-12-00255.1.
50. Lyulyukin, V.; Kallistratova, M.; Kouznetsov, R.; Kuznetsov, D.; Chunchuzov, I.; Chirokova, G. Internal gravity-shear waves in the atmospheric boundary layer from acoustic remote sensing data. *Izvestiya, Atmos. and Ocean. Phys.* **2015**, *51*, 193–202.
51. Argentini, S.; Petenko, I.; Bucci, S.; Mastrantonio, G.; Conidi, A.; Federico, S.; Casasanta, G.; Sozzi, R.; Morelli, M.; Cozzolino, M.; others. LACOST, an atmospheric laboratory on the Tyrrhenian coastline. Ext. Abstr. of presentations from the 18th Intern. Symp. for the Advancement of Boundary-Layer Remote Sensing, 6-9 June 2016, Varna, Bulgaria, 2016.

